Naïve B cell trafficking is shaped by local chemokine availability and LFA-1-independent stromal interactions

Fernanda M. Coelho[1+], Daniela Natale[1+], Silvia F. Soriano[1+], Miroslav Hons[1], Jim Swoger[2], Jürgen Mayer[2], Renzo Danuser[1], Elke Scandella[3], Markus Pieczyk[1], Hans-Günter Zerwes[4], Tobias Junt[4], Andreas W. Sailer[4], Burkhard Ludewig[3], James Sharpe[2], Marc Thilo Figge[5], and Jens V. Stein[1]*

+ Authors contributed equally to this work

* Corresponding author

[1]Theodor Kocher Institute, University of Bern, Bern, Switzerland

[2]EMBL/CRG Systems Biology Research Unit, Centre for Genome Regulation (CRG), Barcelona, Spain

[3]Institute of Immunobiology, Cantonal Hospital St. Gallen St. Gallen, Switzerland

[4]Novartis Institutes for BioMedical Research, Basel, Switzerland

[5] Leibniz Institute for Natural Product Research and Infection Biology – Hans Knöll Institute, Friedrich Schiller University, Jena, Germany

Corresponding author: Jens V. Stein, Ph. D.
Theodor Kocher Institute
University of Bern
Freiestr. 1
3012 Bern
Switzerland
Tel: (+41) 31 631 5390
Fax: (+41) 31 631 3799
Email: jstein@tki.unibe.ch

Word count: 3989

Running title: Chemokine control of naïve B cell migration

Abbreviations: HEV, high endothelial venules; 2PM, twophoton microscopy

Key points (bullet format):

- CXCR5, but not CXCR4 or CCR7, acts with LFA-1 to mediate random B cell migration in T cell area and B cell follicles in resting and inflamed lymph nodes
- In contrast, stromal guidance during B cell migration is LFA-1- and CXCR5-independent

Abstract

It remains unknown how naïve B cells compute divergent chemoattractant signals of the T cell area and B cell follicles during *in vivo* migration. Here, we used twophoton microscopy of peripheral lymph nodes (PLNs) for a comprehensive analysis of the prototype G-protein-coupled receptors (GPCRs) CXCR4, CXCR5, and CCR7 during B cell migration, as well as the integrin LFA-1 for stromal guidance. CXCR4 and CCR7 did not influence parenchymal B cell motility and distribution, despite their role during B cell arrest in venules. In contrast, CXCR5 played a non-redundant role for B cell motility in follicles and in the T cell area. B cell migration in the T cell area followed a random guided walk model, arguing against directed migration *in vivo*. LFA-1 but not α4 integrins contributed to B cell motility in PLN. However, stromal network guidance was LFA-1-independent, uncoupling integrin-dependent migration from stromal attachment. Finally, we observed that despite a 20-fold reduction of chemokine expression in virus-challenged PLNs, CXCR5 remained essential for B cell screening of antigen-presenting cells. Our data provide an overview on the contribution of prototype GPCRs and integrins during naïve B cell migration and shed light on the local chemokine availability that these cells compute.

Introduction

Chemokine receptors and other G-protein-coupled receptors (GPCR) guide naïve lymphocytes into and within lymphoid tissue. Thus, arrest of blood-borne B cells in HEV requires binding of the chemokine receptors CXCR4, CCR7 and to a minor extent CXCR5 to their respective ligands CXCL12, CCL19/CCL21 and CXCL13, leading to LFA-1 activation and binding to ICAM-1 and ICAM-2 [1 2 3]. Studies in mice have uncovered that B cells accumulate from their entry point in the T cell area in one of approximately 7-35 B cell follicles located in the PLN cortex [4,5]. During their migration inside lymphoid tissue, B cells use the ICAM-1-expressing fibroblastic reticular cell (FRC) network of the T cell area and the follicular dendritic cell (FDC) network in follicles as guidance structures [6,7]. Analysis of tissue sections showed that B cell accumulation inside follicles is critically dependent on CXCR5 and CXCL13 production by FDCs [8-10]. Naïve B cells also express moderate levels of Ebi2 (aka GPR183), a GPCR binding 7α,25-dihydroxycholesterol (7α,25-OHC) produced by the cholesterol 25-hydroxylase (CH25H), and which mediates accumulation of B cells to the outer rim of B cell follicles [11-14].

Despite these insights, there are to date remarkably few data how chemokine receptors control active B cell motility within lymphoid tissue. Since naïve B cells express chemokine receptors for both the T cell area and B cell follicles, an attractive hypothesis is that the balanced responsiveness to CCR7 ligands of the T cell area and CXCL13 in B cell follicles shapes dynamic B cell motility and restrains entry of $CXCR5^{-/-}$ B cells into follicles. Yet, how naïve B cells compute the hierarchy and potential redundancy of divergent promigratory factors has remained elusive. This is further complicated by technical limitations regarding the assessment of the actual availability of chemokines on the stromal network. Thus, it remains unclear whether B cells follow a CXCL13 gradient from their point of arrival in the T cell area to enter follicles, or alternatively, whether they display a chemokinetic behavior, an issue directly linked to the presence or absence of CXCL13 gradients attracting B cells to B cell follicles. Also, while it is well established that LFA-1 and its ligand ICAM-1 expressed on stromal cell networks contribute to parenchymal B cell motility [3], it remains unclear whether block of these interactions affects the guidance function of FRCs and FDCs during B cell migration and their microenvironmental distribution. Finally, although homeostatic chemokine levels are strongly suppressed in inflamed PLNs [1,15 2,16], naive B cells retain the capacity to engage with antigen-presenting FDCs through unknown mechanisms [3,17].

Here, we used live twophoton microscopy (2PM) imaging and applied a combined genetic and pharmacologic approach to functionally address chemokine availability and to evaluate the contribution of CXCR5, CCR7 and CXCR4 during dynamic B cell motility, including gradient sensing within the T and B cell areas. Furthermore, we investigated the role for integrins during interactions of B cells with the stromal cell

network. Our data support a non-redundant role for CXCR5 and LFA-1 in mediating rapid non-directed B cell migration without affecting guidance by stromal networks. Despite their well-described role for B cell attachment in HEV, CCR7 and CXCR4 played no role for parenchymal B cell motility or distribution. The remarkably high *in vivo* sensitivity of CXCR5 on naïve B cells allowed interactions with antigen-presenting FDCs even when CXCL13 levels were strongly depressed, thus ensuring effective participation of naïve B cells in ongoing immune reactions.

Methods

Mice

Eight to 12-week-old male and female CXCR5$^{-/-}$ mice [4,5,8], *plt/plt* mice [6,7,18], CCR7$^{-/-}$ mice [8-10,19] and ICAM-1-deficient mice [11-14,20] on the C57BL/6 background were bred at our animal facility (Bern, Switzerland) while Ebi2$^{-/-}$ mice (C57BL/6 strain) and CH25H$^{-/-}$ mice [3,21] on the C57BL/6 background were bred at Novartis (Basel, Switzerland). Sex-and age-matched C57BL/6 mice (Harlan, The Netherlands) were used as wild type lymphocyte donors or recipient mice. For the generation of GFP-expressing stromal bone marrow chimeras, C57BL/6-Tg(CAG-EGFP)1Osb/J (CAG-GFP) were irradiated with 1000 cGy and reconstituted with at least 10 Mio C57BL/6 bone marrow cells. Reconstitution rates after 8 weeks were above 98%. All experiments were performed in accordance with local and federal animal experimentation regulations.

Reagents

CCL21 was from Peprotech (London, UK) and CXCL13 from R&D System (Minneapolis, MN). Fluorescent dyes for cell labeling (CFSE, CellTracker Blue and CellTracker Orange) were purchased from Molecular probes (Eugene, OR). The CXCR4 antagonist NIBR1816 was synthetized as described [22]. Anti-LFA-1 mAb (clone FD441.8) and anti-α4 integrin mAb (clone PS/2) were produced by nanotools (Freiburg, Germany).

Statistical analysis

The student's t-test or ANOVA were used to determine statistical significance (Prism, GraphPad). Statistical significance was set at $p < 0.05$.

All other methods are described in Supplemental Information.

Results

CXCR5 controls B cell follicle entry and migration speed in lymphoid tissue

First, we analyzed the importance of CXCR5 for B cell homing and egress, as well as for entry from the HEV-containing T cell area into B cell follicles. We adoptively transferred fluorescently labeled WT and CXCR5$^{-/-}$ B cells into WT hosts and analyzed their distribution inside entire PLNs using selective plane illumination microscopy, which preserves the 3D organ structure (**Supplemental Figure 1A**). CXCR5 was not required for B cell homing to PLN (**Figure 1A**), in line with abundant CCL21 presentation on HEVs (**Supplemental Figure 1B and C**). Similarly, CXCR5 had only a minor, non-significant effect on the dwell time of B cells inside lymphoid tissue, as determined by blocking further homing using Mel-14 (**Figure 1A**). As reported [8], lack of CXCR5 prevented B cell entry into follicles and retained them in close vicinity of the HEV vascular network, in a distribution similar to T cells (**Figure 1B and C**). Thus, CXCR5 deficiency in B cells did not result in a homogeneous distribution pattern of random positions throughout T cell areas and B cell follicles, but consistently excluded mutant B cells from follicles, where CXCL13 is produced (**Supplemental Figure 1D**).

We next investigated to which degree lack of CXCR5 impaired dynamic B cell motility and, as a consequence, entry into follicles, using 2PM and anatomical landmarks for HEV (= T cell area) and B cell follicles, respectively (**Figure 1D and Supplemental movie 1**). The labeling for HEV allowed us furthermore discarding tracks in the perivascular space, where migration is lower than in the parenchyma [3 5]. While the track distribution analysis confirmed that CXCR5 was required for efficient entry into the follicular microenvironment, occasional CXCR5$^{-/-}$ B cells were observed inside follicles (**Figure 1E and F**). There, CXCR5 contributed to B cell migration speed (8.3 ± 2.6 μm/min for WT B cells versus 6.8 ± 2.8 μm/min for CXCR5$^{-/-}$ B cells; $p<0.0001$) and low turning angles (**Figure 1G and H**). Accordingly, the motility coefficient was reduced from 18.2 μm^2/min for WT B cells by more than 50% to 8.2 μm^2/min for CXCR5$^{-/-}$ B cells (**Figure 1I**).

WT and CXCR5$^{-/-}$ B cells moving in the T cell area showed a robust motility and moved only marginally slower than in B cell follicles. Unexpectedly, we again found WT B cells to move with increased speed and directionality compared to CXCR5$^{-/-}$ B cells (7.7 ± 2.9 μm/min for WT B cells versus 6.9 ± 2.6 μm/min for CXCR5$^{-/-}$ B cells; $p<0.003$; **Figure 1G and H**), resulting in a 26% decrease of the motility coefficient in the absence of CXCR5 (14.9 versus 11.0 μm^2/min, respectively; **Figure 1I**). In summary, CXCR5 contributes not only to B cell entry into the follicular microenvironment, but also to the migration speed and narrow turning angles inside the T cell area.

Lack of CCR7 and CXCR4 signaling does not alter dynamic B cell behavior within lymphoid tissue

The robust migration of CXCR5$^{-/-}$ B cells inside the T cell area pointed to additional factors that drive B cell motility. B cells express CCR7 [23] and show a strong chemotactic response *in vitro* to CCL21 (**Figure 2A**), which promotes LFA-1 activation in HEV [1 5]. Similarly, B cells respond to CXCL12 with strong migration, which can be blocked by the CXCR4 antagonist NIBR1816 (**Figure 2B**) [22]. We first examined whether CCR7 might propel B cells within the T cell area and retain B cells in this microenvironment, thereby inhibiting random entry of CXCR5$^{-/-}$ B cells into follicles. We used *plt/plt* mice, which lack expression of CCL19 and CCL21 in the T cell area of PLNs [7,24], as recipients and followed the dynamic migration of adoptively transferred WT and CXCR5$^{-/-}$ B cells using 2PM as in Figure 1. Despite the lack of CCR7 ligands in the T cell area, we observed a similar distribution of WT and CXCR5$^{-/-}$ B cell as in WT PLNs (**Figure 2C and D**). Furthermore, the speeds of WT and CXCR5$^{-/-}$ B cells were comparable to the ones observed in WT PLNs, with CXCR5$^{-/-}$ B cells showing a robust but slower migration than WT B cells (T cell area: WT, 8.4 ± 2.9 μm/min vs. CXCR5$^{-/-}$, 7.3 ± 2.7 μm/min, $p<0.0001$; B cell follicle: WT, 7.8 ± 2.7 μm/min vs. CXCR5$^{-/-}$, 6.3 ± 2.2 μm/min; $p<0.01$; **Supplemental movie 2**). We confirmed the lack of a detectable influence of CCR7 on B cell accumulation in follicles or migration parameters using CCR7$^{-/-}$ B cells in WT PLNs (**Supplemental Figure 2** and data not shown) .

We next investigated potential redundancy of CXCR5, CCR7 and CXCR4 for B cell motility by treating *plt/plt* mice with NIBR1816. Experiments were timed such that high levels of NIBR1816 were present at the time of imaging inside PLNs: the compound levels achieved were 771 ± 42 nM in blood and 33.1 ± 7.2 μg/g tissue in lymph nodes, levels at which marked inhibition of CXCR4 is expected [22]. Nonetheless, the dynamic migration parameters of WT and CXCR5$^{-/-}$ B cells, as well as their microenvironmental distribution, were not altered through the combined lack of CCR7 and CXCR4 signals, although we observed fewer CXCR5$^{-/-}$ B cells in B cell follicles in this set of experiments (**Figure 2F and G**). In summary, our 2PM data do not support a role for CXCR4 or CCR7 ligands during parenchymal B cell migration, or retention in this microenvironment, which suggests a limited availability of these chemokines for migrating B cells. This either points to an inherent capacity of B cells to be motile on stromal support in the absence of such signals, or to additional chemokinetic signals for B cells in lymphoid organs.

To address the latter point, we analyzed the role of the recently described GPCR Ebi2 during naïve B cell migration in WT PLNs. As predicted from previous data from histological sections [11,12], 2PM data showed that Ebi2$^{-/-}$ B cells interacted efficiently with CD35^{+} FDC network, while a higher percentage of WT B cell tracks were located in the outer rim of B cell follicles (**Supplemental Figure 3A and B**). Since CH25H is involved in the production of the major Ebi2 ligand 7α,25-OHC, we transferred WT and Ebi2$^{-/-}$ B cells into

CH25H$^{-/-}$ hosts predicting to observe a comparable association of both cell populations with the CD35^{+} FDC network. Instead, WT B cells were still found in larger numbers in the outer B cell follicle rim as compared to Ebi2$^{-/-}$ B cells (**Supplemental Figure 3C and D**), which migrated faster in B cell follicles as compared to WT B cells (8.3 ± 2.7 µm/min for WT B cells versus 9.4 ± 4.0 µm/min for Ebi2$^{-/-}$ B cells; $p<0.0001$). Our data suggest therefore that under steady-state conditions, Ebi2 controls dynamic naïve B cell distribution to the outer B cell follicle rim, without acting as a promigratory factor. Our data also suggest that in the absence of an inflammatory signal, there is a second source of 7α,25-OHC independent of CH25H (**Supplemental Figure 3E**).

Non-directional B cell migration within the T cell area results in delayed entry into follicles

The faster migration of WT B cells in the T cell area as compared to CXCR5$^{-/-}$ B cells (**Figures 1G, 2E and 2G**) pointed to the presence of functional CXCL13 inside the T cell area. We therefore analyzed whether after entering the T cell area through HEV, B cells migrated in a directed manner towards adjacent follicles, i.e. areas that express high levels of CXCL13. Since in individual 2PM recordings the number of analyzable B cell tracks inside the T cell area was too low for a meaningful statistical evaluation of directionality, while the relative position of B cell follicles and T cell area varied between recordings, we developed a method to normalize B cell tracks from different image sequences. For each B cell track in the T cell area, we determined the closest (x,y) coordinates of adjacent B cell follicles relative to the starting position of the track (**Figure 3A**)**.** Normalizing these (x,y) coordinates to the 12 o'clock position allowed aligning tracks from numerous movies for detection of subtle chemotactic effects. However, within the limits of the observation period and tissue volume, we did not detect evidence for directional B cell migration from the T cell area towards adjacent B cell follicles (**Figure 3B and Supplemental Figure 4**). The percentage of B cells migrating within a 120º angle from their track origin towards the closest follicle intersection was 23.5% for WT B cells, and 25.5% for CXCR5$^{-/-}$ B cells as negative control. These data suggest that a long-range CXCL13 gradient in the T cell area is not detectable.

Next, we analyzed whether recent B cell immigrants to PLNs located in close proximity to B cell follicles experienced a short-range chemotactic CXCL13 gradient for efficient follicle entry. GFP-expressing B cells were transferred into mice that had previously received both WT B cells and anti-CD35 mAb to outline entire B cell follicles and the inner FDC network, respectively. B cells accumulated over the time course of 2-3 h post transfer in B cell follicles (**Figure 3C**). When analyzing B cell behavior in close proximity to B cell follicles, we found that a majority of B cells, instead of readily entering B cell follicles, turned back to the T cell area (**Figure 3D and Supplemental movies 3 and 4**). In average, only one out of four B cells in close

proximity to follicles was observed to directly enter from the T cell area (**Figure 3F**), suggesting additional molecular or anatomical constraints for cell entry into follicles. Taken together, although B cells eventually accumulate in follicles, we were unable to detect preferential migration towards follicles.

LFA-1 and CXCR5 cooperate during B cell motility without affecting guidance by the lymphoid stromal network

Since in addition to chemokine receptors, integrins are involved in dynamic B cell migration within lymphoid tissue [3], we investigated the role of the B cell-expressed adhesion molecules LFA-1 and α4 integrins during B cell-stromal network interactions *in vivo*. As reported [3], LFA-1 blocking resulted in decreased WT B cell speed within B cell follicles from 8.3 ± 2.6 µm/min (**Figure 1G**) to 6.0 ± 2.6 µm/min (**Figure 4A**). Similarly, B cell speed within the T cell area was decreased from 7.7 ± 2.9 to 5.8 ± 2.4 µm/min for WT B cells, and from 6.9 ± 2.6 to 5.2 ± 2.0 µm/min for CXCR5$^{-/-}$ B cells after LFA-1 blockade (**Figure 4A**). Although this decrease seems modest, breathing and tissue deformability artifacts make the *in vivo* measurements of lymphocyte speeds below 5 µm/min difficult [25,26]. A more robust readout is the motility coefficient, which dropped to 3.3 µm^2/min for CXCR5$^{-/-}$ B cells in the T cell area after LFA-1 blocking. Additional blocking of α4 integrins in combination with CXCR4 antagonist treatment in *plt/plt* mice did not result in a further decrease of B cell migration speeds (**Figure 4B**), supporting a non-redundant role for LFA-1 and CXCR5 controlling naive B cell migration. In contrast, we did not observe an effect of the functional absence of LFA-1 or its main ligand ICAM-1 on WT, CCR7$^{-/-}$ and CXCR5$^{-/-}$ B cell distribution, arguing against a role for integrins and T cell zone chemokines during B cell follicle compartmentalization (**Supplemental Figure 5**).

Since stromal cells express high levels of ICAM-1 [6], the decreased migration speed observed in the absence of functional LFA-1 may be due to defective adhesion of B cells to the underlying stromal network. We tested this hypothesis using bone marrow chimeras expressing GFP in the stromal compartment as recipients for fluorescently labeled WT and CXCR5$^{-/-}$ B cells, followed by 2PM analysis as described [7]. We found that adoptively transferred WT and CXCR5$^{-/-}$ B cells remained attached during their migration to the stromal network, and the vast majority of turns was in association with GFP$^+$ fibers (**Figure 4C and D; Supplemental movies 5 and 6**). Yet, B cell guidance by the stromal network was unaffected by LFA-1 blockade, both for WT and CXCR5$^{-/-}$ B cells in the T cell area and for WT B cells migrating along the FDC network (**Figure 4C and D; Supplemental movies 7 and 8**). In summary, LFA-1-ICAM-1 interactions cooperate with CXCR5 signaling to warrant efficient B cell motility, but are not required for guidance by the lymphoid stromal network.

CXCR5-dependent naïve B cell accumulation in dispersed B cell clusters during viral infection

Our data support a model in which CXCR5 is the predominant GPCR accelerating B cells under homeostatic conditions, while Ebi2 directs B cell localization to the outer rim, and CCR7 and CXCR4 are irrelevant for parenchymal B cell motility or compartmentalization. Infection of mice with lymphocytic choriomeningitis virus (LCMV) results in a strong disruption of the normal lymphoid architecture with a concomitant decrease in the expression of homeostatic chemokines including CXCL13 [15,16]. Using Optical Projection Tomography [4] and qPCR analysis, we confirmed the LCMV-induced severe disruption of B cell follicles into small or large, unevenly shaped B cell clusters, accompanied by strongly decreased expression levels of CXCL12, CXCL13 and CH25H but not Ebi2 and Cyp7b1, an enzyme involved in production of oxysterols (**Figure 5A and B**). We then investigated how this altered chemokine landscape affects motility parameters and FDC interactions of non-activated B cells. Using 2PM at day 11 post infection, we observed a preferential WT B cell migration on small and large B cell clusters as identified by $CD35^{+}$ FDCs, which likely represent the light zones of ongoing germinal center reactions (**Figure 5C**). In contrast, $CXCR5^{-/-}$ B cells were mostly excluded from B cell clusters and rarely interacted with FDC despite a 95% reduction of CXCL13 mRNA levels (**Figure 5C and D**). The ability of naïve B cells to screen FDC for cognate antigen and to engage in ongoing immune reactions therefore depends on CXCL13 sensing over a wide range of expression levels. Similar to non-inflamed PLN, the rare $CXCR5^{-/-}$ B cells in B cell clusters migrated slower than WT B cells (**Figure 5E**). Taken together, our data uncover an unexpectedly high CXCR5-dependent sensitivity to enable B cell accumulation in B cell clusters in severely disrupted PLNs, thus ensuring continuous scanning of antigen-presenting FDCs by naïve B cells.

Discussion

B cells express GPCRs for chemokines presented on the HEV lumen, the T cell area and B cell follicles, and which are able to efficiently induce directed migration in controlled *in vitro* experiments. How motile B cells compute various overlapping, divergent chemokine sources *in vivo* has remained unknown, also since chemokine availability and gradients are intrinsically difficult to detect. We used naive WT and mutant B cells as surrogate "biosensors" to deduce from their dynamic migratory behavior the shape and availability of chemoattractants gradients in lymphoid tissue. Using 2PM imaging and a combined pharmacological and genetic inhibition approach, our image analysis data dissect the contributions of the prototypical chemokine receptors CXCR4, CXCR5 and CCR7 for B cell migration inside lymphoid tissue to uncover the factors that migrating B cells are able to compute during immunosurveillance. Our data provide a "chemokine" landscape as seen by naive B cells and uncover an integrin-independent guidance function for FRC and FDC stromal networks (**Supplemental Figure 6**).

CXCR4 and CCR7 ligands are highly expressed in lymphoid tissue, and B cell adhesion in HEV is efficiently mediated by CCL21 and CXCL12 [1]. In contrast, our 2PM analysis showed that CCR7 and CXCR4 signaling did not alter motility parameters or distribution of B cells after transmigration into PLN parenchyme, whereas CCR7 increases T cell migration by approximately 30% [25,27-29]. The compartmentalized response of naive B cells to HEV- but not FRC-presented CCL21 is likely due to increased CCL21 deposition on the vasculature as compared to parenchyme. Since non-activated B cells express lower CCR7 levels than T cells, our data suggest that outside HEV, B cells are unable to detect the physiologically available levels of T cell area-expressed chemokines. As chemokines are in part synthesized by lymphoid stromal cells including FRCs, CCL21 detected in tissue sections could be preferentially localized inside FRC conduits for transport to the HEV network, where it may contribute to lymphocyte recruitment [30 31 32 33 34]. Thus, 2PM imaging helps to uncouple *in vitro* from *in vivo* chemoattractant responsiveness, which depends on the "usable" chemokine levels available to trafficking lymphocytes. At the same time, these data highlight the importance for chemokine receptor levels for responding to presumably limited amounts of stromal chemokine.

In contrast to CXCR4 and CCR7, CXCR5 increased the migration speed of WT B cells localized in the T cell area as well as in B cell follicles. Although it is intuitive to assume that B cells would follow a chemotactic gradient from their site of entry in the T cell zone towards adjacent B cell follicle, as recently observed during DC migration to lymphatic vessels [35 36], we did not find evidence for directed motility inside lymphoid tissue. While we cannot exclude a subtle follicle-directed B cell taxis undetectable due to the confined observation volume and duration [37], B cells in close proximity to follicles typically turned back into the T cell area, similar to observations made by Kehrl and colleagues [5]. This may be due to one or several of the following

scenarios: subsets of stromal cells in the T cell area express CXCL13 [38], which may present low levels of CXCL13 in the T cell area, thereby disrupting a chemotactic gradient. However, in immunofluorescent sections, virtually all detectable CXCL13 is found in B cell follicles. As a second option, secreted CXCL13 may diffuse from follicles into the adjacent T cell area in a process reminiscent of cytokine permeation throughout reactive PLNs [39]. Since T cells in the adjacent T cell area are highly motile and ignore the released CXCL13, a gradient may be unstable due to constant stirring of the extracellular fluid and could explain the chemokinetic effect observed here. A third possibility may be linked to the underlying stromal network anatomy, in particular the cortical ridge consisting of dense ERTR7-positive reticular fibers surrounding B cell follicles [40]. In this scenario, B cells migrating close to follicles lack appropriate guidance structures to lead them into the B cell area. Furthermore, the tightly packed environment of B cell follicles may constitute a physical obstacle for randomly migrating lymphocytes. Thus, successful entry into follicles would require stochastic encounters with stromal elements leading to the FDC network, and CXCL13 signaling to provide the attractive energy to allow entry into the dense B cell population. Future studies are required to clarify the mechanisms underlying the remarkable separation of T cells and B cells and explain why cells lacking CXCR5 expression do not randomly enter B cell follicles, even in the absence of presumed T cell area retention signals. Additional molecules, presumably ligands for GPCRs due to the dependence of B cell migration on Gαi2 [41], or novel adhesion molecules likely contribute to B cell migration in lymphoid tissue and retention of CXCR5$^{-/-}$ B cells in the T cell area. From our *in vivo* analysis, we can exclude CCR7, CXCR4, ICAM-1, LFA-1 and α4 integrins from participating in B cell retention in the T cell area. A potential candidate is B cell-expressed CLEC-2, which binds podoplanin expressed on FRC [42]. Future studies are required to address these issues.

The startling high sensitivity of naïve B cells to low levels of CXCL13 in the T cell area is reflected under inflammatory conditions. Using a virus infection model, our data showed that CXCR5 was absolutely required to enable naïve B cell screening of antigen-loaded FDCs, despite strongly suppressed CXCL13 expression. A possible explanation for these observations could be the decisive influence of chemokine receptor levels for chemokine detection *in vivo*, i.e. only cells above a high chemokine receptor expression threshold are able to successfully sense or compete with other leukocytes for chemokines with low availability. In any event, the ability of naïve B cells to respond to CXCL13 over a wide range of expression levels defines CXCR5 as a key player in the engagement of naïve B cells in ongoing germinal centers, where they can compete with previously activated B cells for antigen deposited on FDCs [17].

Acknowledgements

We thank U.H. von Andrian and Sarah Henrickson for MatLab scripts, Bettina Stolp, Aleksandra Ozga and Matthias Baumann for help with experiments, Britta Engelhardt for continuous support, and the Novartis colleagues Agnes Feige, Noemie Beluch, Inga Preuss, Thomas Suply, Isabelle Christen and Juan Zhang for preparation and mass spectrometry analysis of tissue samples, and Christian Beerli for analysis of NIBR levels. This project was supported by Sinergia grants CRSII3-125447 and -141918 (to BL, JS and JVS), SNF grant 31003A_135649 (to JVS) and the VIBRANT project 228933/FP7-NMP (to JS).

Authorship contribution

FMC, DN, SFS, MH, JSw, JM, RD, ES, MP, HGZ and JVS performed experiments and analyzed the data. ES, TJ, and AWS provided vital material. MTF performed the single cell tracking analysis. BL, JS and JVS supervised the work. FCM, DN, SFS and JVS wrote the manuscript with feedback from all authors.

Conflict of Interest Disclosure

The authors declare no conflict of interest.

References

1. Okada T, Ngo VN, Ekland EH, et al. Chemokine requirements for B cell entry to lymph nodes and Peyer's patches. *J Exp Med*. 2002;196(1):65–75.
2. Ebisuno Y, Tanaka T, Kanemitsu N, et al. Cutting edge: the B cell chemokine CXC chemokine ligand 13/B lymphocyte chemoattractant is expressed in the high endothelial venules of lymph nodes and Peyer's patches and affects B cell trafficking across high endothelial venules. *J Immunol*. 2003;171(4):1642–1646.
3. Boscacci RT, Pfeiffer F, Gollmer K, et al. Comprehensive analysis of lymph node stroma-expressed Ig superfamily members reveals redundant and nonredundant roles for ICAM-1, ICAM-2, and VCAM-1 in lymphocyte homing. *Blood*. 2010;116(6):915–925.
4. Kumar V, Scandella E, Danuser R, et al. Global lymphoid tissue remodeling during a viral infection is orchestrated by a B cell-lymphotoxin-dependent pathway. *Blood*. 2010;115(23):4725–4733.
5. Park C, Hwang I-Y, Sinha RK, et al. Lymph node B lymphocyte trafficking is constrained by anatomy and highly dependent upon chemoattractant desensitization. *Blood*. 2012;119(4):978–989.
6. Woolf E, Grigorova I, Sagiv A, et al. Lymph node chemokines promote sustained T lymphocyte motility without triggering stable integrin adhesiveness in the absence of shear forces. *Nat Immunol*. 2007;8(10):1076–1085.
7. Bajénoff M, Egen JG, Koo LY, et al. Stromal cell networks regulate lymphocyte entry, migration, and territoriality in lymph nodes. *Immunity*. 2006;25(6):989–1001.
8. Förster R, Mattis AE, Kremmer E, et al. A putative chemokine receptor, BLR1, directs B cell migration to defined lymphoid organs and specific anatomic compartments of the spleen. *Cell*. 1996;87(6):1037–1047.
9. Ansel KM, Ngo VN, Hyman PL, et al. A chemokine-driven positive feedback loop organizes lymphoid follicles. *Nature*. 2000;406(6793):309–314.
10. Cyster JG. B cell follicles and antigen encounters of the third kind. *Nat Immunol*. 2010;11(11):989.
11. Pereira JP, Kelly LM, Xu Y, Cyster JG. EBI2 mediates B cell segregation between the outer and centre follicle. *Nature*. 2009;460(7259):1122–1126.
12. Gatto D, Paus D, Basten A, Mackay CR, Brink R. Guidance of B Cells by the Orphan G Protein-Coupled Receptor EBI2 Shapes Humoral Immune Responses. *Immunity*. 2009;31(2):259–269.
13. Hannedouche S, Zhang J, Yi T, et al. Oxysterols direct immune cell migration via EBI2. *Nature*. 2011;475(7357):524.
14. Liu C, Yang XV, Wu J, et al. Oxysterols direct B-cell migration through EBI2. *Nature*. 2011;475(7357):519.
15. Mueller SN, Hosiawa-Meagher KA, Konieczny BT, et al. Regulation of homeostatic chemokine expression and cell trafficking during immune responses. *Science*. 2007;317(5838):670–674.
16. Scandella E, Bolinger B, Lattmann E, et al. Restoration of lymphoid organ integrity through the interaction of lymphoid tissue-inducer cells with stroma of the T cell zone. *Nat Immunol*. 2008;9(6):667–675.
17. Schwickert TA, Lindquist RL, Shakhar G, et al. In vivo imaging of germinal centres reveals a dynamic open structure. *Nature*. 2007;446(7131):83–87.
18. Nakano H, Tamura T, Yoshimoto T, et al. Genetic defect in T lymphocyte-specific homing into peripheral lymph nodes. *Eur J Immunol*. 1997;27(1):215–221.

19. Förster R, Schubel A, Breitfeld D, et al. CCR7 coordinates the primary immune response by establishing functional microenvironments in secondary lymphoid organs. *Cell*. 1999;99(1):23–33.
20. Xu H, Gonzalo JA, St Pierre Y, et al. Leukocytosis and resistance to septic shock in intercellular adhesion molecule 1-deficient mice. *J Exp Med*. 1994;180(1):95–109.
21. Bauman DR, Bitmansour AD, McDonald JG, et al. 25-Hydroxycholesterol secreted by macrophages in response to Toll-like receptor activation suppresses immunoglobulin A production. *Proceedings of the National Academy of Sciences*. 2009;106(39):16764–16769.
22. Thoma G, Streiff MB, Kovarik J, et al. Orally Bioavailable Isothioureas Block Function of the Chemokine Receptor CXCR4 In Vitro and In Vivo. *J. Med. Chem.* 2008;51(24):7915–7920.
23. Kim CH, Pelus LM, White JR, et al. CK beta-11/macrophage inflammatory protein-3 beta/EBI1-ligand chemokine is an efficacious chemoattractant for T and B cells. *J Immunol*. 1998;160(5):2418–2424.
24. Gunn MD, Kyuwa S, Tam C, et al. Mice lacking expression of secondary lymphoid organ chemokine have defects in lymphocyte homing and dendritic cell localization. *J Exp Med*. 1999;189(3):451–460.
25. Faroudi M, Hons M, Zachacz A, et al. Critical roles for Rac GTPases in T cell migration to and within lymph nodes. *Blood*. 2010.
26. Nombela-Arrieta C, Mempel TR, Soriano SF, et al. A central role for DOCK2 during interstitial lymphocyte motility and sphingosine-1-phosphate-mediated egress. *J Exp Med*. 2007;204(3):497–510.
27. Okada T, Cyster J. CC chemokine receptor 7 contributes to Gi-dependent T cell motility in the lymph node. *The Journal of Immunology*. 2007;178(5):2973.
28. Worbs T, Mempel TR, Bölter J, Andrian Von UH, Förster R. CCR7 ligands stimulate the intranodal motility of T lymphocytes in vivo. *J Exp Med*. 2007;204(3):489–495.
29. Asperti-Boursin F, Real E, Bismuth G, Trautmann A, Donnadieu E. CCR7 ligands control basal T cell motility within lymph node slices in a phosphoinositide 3-kinase-independent manner. *J Exp Med*. 2007;204(5):1167–1179.
30. Baekkevold ES, Yamanaka T, Palframan RT, et al. The CCR7 ligand elc (CCL19) is transcytosed in high endothelial venules and mediates T cell recruitment. *J Exp Med*. 2001;193(9):1105–1112.
31. Link A, Vogt T, Favre S, et al. Fibroblastic reticular cells in lymph nodes regulate the homeostasis of naive T cells. *Nat Immunol*. 2007;8(11):1255–1265.
32. Bai Z, Hayasaka H, Kobayashi M, et al. CXC chemokine ligand 12 promotes CCR7-dependent naive T cell trafficking to lymph nodes and Peyer's patches. *J Immunol*. 2009;182(3):1287–1295.
33. Kanemitsu N, Ebisuno Y, Tanaka T, et al. CXCL13 is an arrest chemokine for B cells in high endothelial venules. *Blood*. 2005;106(8):2613–2618.
34. Frontera V, Arcangeli M-L, Zimmerli C, et al. Cutting Edge: JAM-C Controls Homeostatic Chemokine Secretion in Lymph Node Fibroblastic Reticular Cells Expressing Thrombomodulin. *J Immunol*. 2011;187(2):603–607.
35. Tal O, Lim HY, Gurevich I, et al. DC mobilization from the skin requires docking to immobilized CCL21 on lymphatic endothelium and intralymphatic crawling. *J Exp Med*. 2011.
36. Weber M, Hauschild R, Schwarz J, et al. Interstitial Dendritic Cell Guidance by Haptotactic Chemokine Gradients. *Science*. 2013;339(6117):328–332.
37. Textor J, Peixoto A, Henrickson SE, et al. Defining the quantitative limits of intravital two-photon lymphocyte tracking. *Proceedings of the National Academy of Sciences*. 2011;108(30):12401–12406.

38. Malhotra D, Fletcher AL, Astarita J, et al. Transcriptional profiling of stroma from inflamed and resting lymph nodes defines immunological hallmarks. *Nat Immunol*. 2012;13(5):499.
39. Perona-Wright G, Mohrs K, Mohrs M. Sustained signaling by canonical helper T cell cytokines throughout the reactive lymph node. *Nat Immunol*. 2010;11(6):520–526.
40. Katakai T, Hara T, Lee J-H, et al. A novel reticular stromal structure in lymph node cortex: an immuno-platform for interactions among dendritic cells, T cells and B cells. *Int Immunol*. 2004;16(8):1133–1142.
41. Han S-B, Moratz C, Huang N-N, et al. Rgs1 and Gnai2 regulate the entrance of B lymphocytes into lymph nodes and B cell motility within lymph node follicles. *Immunity*. 2005;22(3):343–354.
42. Acton SE, Astarita JL, Malhotra D, et al. Podoplanin-rich stromal networks induce dendritic cell motility via activation of the C-type lectin receptor CLEC-2. *Immunity*. 2012;37(2):276–289.

Figure legends

Figure 1. CXCR5 determines localization and migration speed in B cell follicles and T cell area. A. PLN homing and egress of WT and CXCR5$^{-/-}$ B cells. Each dot represents the ratio of WT and CXCR5$^{-/-}$ B cells from pooled PLNs of one recipient mouse before and 12 h after Mel-14 treatment. **B.** 3D reconstruction of a part of the SPIM-scanned PLN shown in Supplemental Figure 1. Asterisks depict accumulation of WT B cells in areas lacking HEV representing B cell follicles, arrows highlight the close association of CXCR5$^{-/-}$ B cells with HEV. Grid length, 123 µm. **C.** Euclidian distance analysis of WT and CXCR5$^{-/-}$ B cells to the nearest HEV. CXCR5$^{-/-}$ B cells are in average closer to HEV located in the T cell area (31 vs. 61 µm), similar to adoptively transferred T cells (39 µm; not shown). **D.** Schematic outline of the 2PM experiments with anatomical landmarking. WT B cells (blue) and MECA-79-Alexa633 were used to delineate the B cell follicle and HEV of the T cell area, respectively. Low amounts of WT and CXCR5$^{-/-}$ B cells were transferred for cell tracking. **E.** Example of 2PM image (top left panel) and microenvironmental classification (top right panel). Individual WT (bottom left panel) and CXCR5$^{-/-}$ (bottom right panel) B cell tracks are depicted. Scale bar, 40 µm. **F.** Percentage of microenvironmental track distribution as determined by 2PM. **G.** Track speeds of WT and CXCR5$^{-/-}$ B cells in T cell area and B cell follicle. Each dot represents an individual track. The red bar represents the mean. **H.** Turning angle distribution of WT and CXCR5$^{-/-}$ B cells in T cell area and B cell follicle. **I.** Motility coefficients of WT and CXCR5$^{-/-}$ B cells in T cell area and B cell follicles. Data in F-I are pooled from 7 mice, 12 image sequences, 697 WT and 591 CXCR5$^{-/-}$ B cell tracks. Fo, B cell follicle; H, HEV; T, T cell area. ** = $p<0.01$, *** = $p<0.001$.

Figure 2. Normal B cell motility and distribution in the absence of CCR7 and CXCR4 signaling. A. Chemotaxis of WT, CXCR5$^{-/-}$ and CCR7$^{-/-}$ B cells towards CXCL13 and CCL21 (100 nM). Data are pooled from duplicates of two independent experiments and shown as mean ± SEM. * = $p < 0.05$; *** = $p < 0.001$ (ANOVA). **B.** Chemotaxis of WT B cells to 100 nM CXCL12, in the presence or absence of NIBR1816 (10 µM). Data are from one experiment in duplicates. **C.** Example of 2PM image (top left panel) and microenvironmental classification (top right panel) in a *plt/plt* PLN. Individual WT (bottom left panel) and CXCR5$^{-/-}$ (bottom right panel) B cell tracks are depicted. Scale bar, 50 µm. **D.** Percentage of microenvironmental track distribution in *plt/plt* PLNs as determined by 2PM. **E.** Speeds of WT and CXCR5$^{-/-}$ B cells in T cell area and B cell follicles in *plt/plt* PLNs. Each dot represents an individual track. The red bar represents the mean. **F.** Percentage of microenvironmental track distribution in NIBR1816-treated *plt/plt* PLNs as determined by 2PM. **G.** Speeds of WT and CXCR5$^{-/-}$ B cells in T cell area and B cell follicles in NIBR1816-treated *plt/plt* PLNs. Each dot represents an individual track. The red bar represents the mean.

Data in D and E are pooled from 3 mice/10 image sequences /558 WT and 263 CXCR5$^{-/-}$ B cell tracks. Data in F and G are from n = 3 mice/5 image sequences /1168 WT and 414 CXCR5$^{-/-}$ B cell tracks. Fo, B cell follicle; H, HEV; T, T cell area. ** = p<0.01, *** = p<0.001.

Figure 3. Absence of a long-or short range CXCL13-mediated directional B cell migration into B cell follicles. A. Schematic outline of the normalization protocol to pool tracks from various 2PM image sequences. **B.** Normalized tracks of WT (left panel) and CXCR5$^{-/-}$ (right panel) B cells migrating in the T cell area. A total of 162 WT and 106 CXCR5$^{-/-}$ B cell tracks are pooled and presented such that the closest intersection point with the nearest B cell follicle at the onset of cell tracking is at the 12 o'clock position. The percentage of tracks falling into a 120° angle towards B cell follicles (dashed lines) is indicated. **C.** Example of 2PM image at indicated times post B cell transfer. Lines define B cell follicles. The dotted squares are shown enlarged in D and E. Scale bar, 50 µm. **D.** 2PM image of B cells migrating parallel to and away from an adjacent B cell follicle taken from the dotted outline from the left panel in C. The top panel shows the starting point of the B cells at the onset of the recording, adjacent to a B cell follicle. Time in min and s. **E.** 2PM image of a B cell track migrating into an adjacent B cell follicle taken from the dotted outline from the middle panel in C. **F.** Frequency of WT B cell tracks either entering or moving parallel to/away from adjacent B cell follicles. All tracks (n = 23) were recorded within the first 150 min after B cell transfer between 20 and 130 µm depth. Fo, B cell follicle.

Figure 4. CXCR5 and functional LFA-1 control B cell speed but are dispensable for B cell guidance by the stromal network. A. Speeds of WT and CXCR5$^{-/-}$ B cells in T cell area and B cell follicle of FD441.8-treated PLNs. Each dot represents an individual track. The red bar represents the mean. Data in A is from 3 mice, 3 image sequences, 534 WT and 227 CXCR5$^{-/-}$ B cell tracks. **B.** Speeds of WT and CXCR5$^{-/-}$ B cells in T cell area and B cell follicle of FD441.8-, PS/2-, and NIBR1816-treated *plt/plt* PLNs. Each dot represents an individual track. The red bar represents the mean. Data in B is from 2 mice, 5 image sequences, 773 WT and 155 CXCR5 $^{-/-}$ B cell tracks. **C.** Example of 2PM images at indicated times post B cell transfer. WT and CXCR5$^{-/-}$ B cells with or without FD441.8-treatment migrate in close association with GFP fibers of the T cell area. The tracks are represented by the dotted line in each frame. Scale bar, 10 µm. **D.** Percentage of motile B cell turn of WT and CXCR5$^{-/-}$ B cells in T cell area and WT B cell in B cell follicle with/without FD441.8-treatment. Data are pooled from 29-63 individual cell tracks. ** = p<0.01. n.s., non significant.

Figure 5. Residual CXCL13 expression suffices for naïve B cell screening of FDCs in virus-challenged PLNs. A. Example of OPT images of WT (control, left) and LCMV-infected (right) PLN on day 8 post infection. The MECA-79^{+} HEV network is in red, and B220^{+} B follicles are green. Scale bar, 1 mm. **B.** CXCL12, CXCL13, Cyb7b1, CH25H and Ebi2 mRNA levels determined by qPCR on day 8 post infection. Each dot represents an individual PLN. The red bar represents the mean. Levels of CXCL12, CXCL13 and CH25H mRNA are significantly reduced as compared to day 0 ($p<0.0001$), as well as mRNA levels of Ebi2 ($p<0.001$) and Cyp7b1 ($p<0.01$). **C.** Example of 2PM image of LCMV-infected PLN. Arrowheads depict CXCR5$^{-/-}$ B cells located at the edge or outside large and small B cell clusters identified by CD35^{+} FDCs. Scale bar, 30 µm. **D.** Percentage of microenvironmental track distribution as determined by 2PM. **E.** Speeds of WT and CXCR5$^{-/-}$ B cells inside CD35^{+} clusters. Each dot represents an individual track. The red bar represents the mean. Data in D-E are pooled from 4 mice, 7 image sequences, 1049 WT and 176 CXCR5 $^{-/-}$ B cell tracks. *** = $p<0.001$.

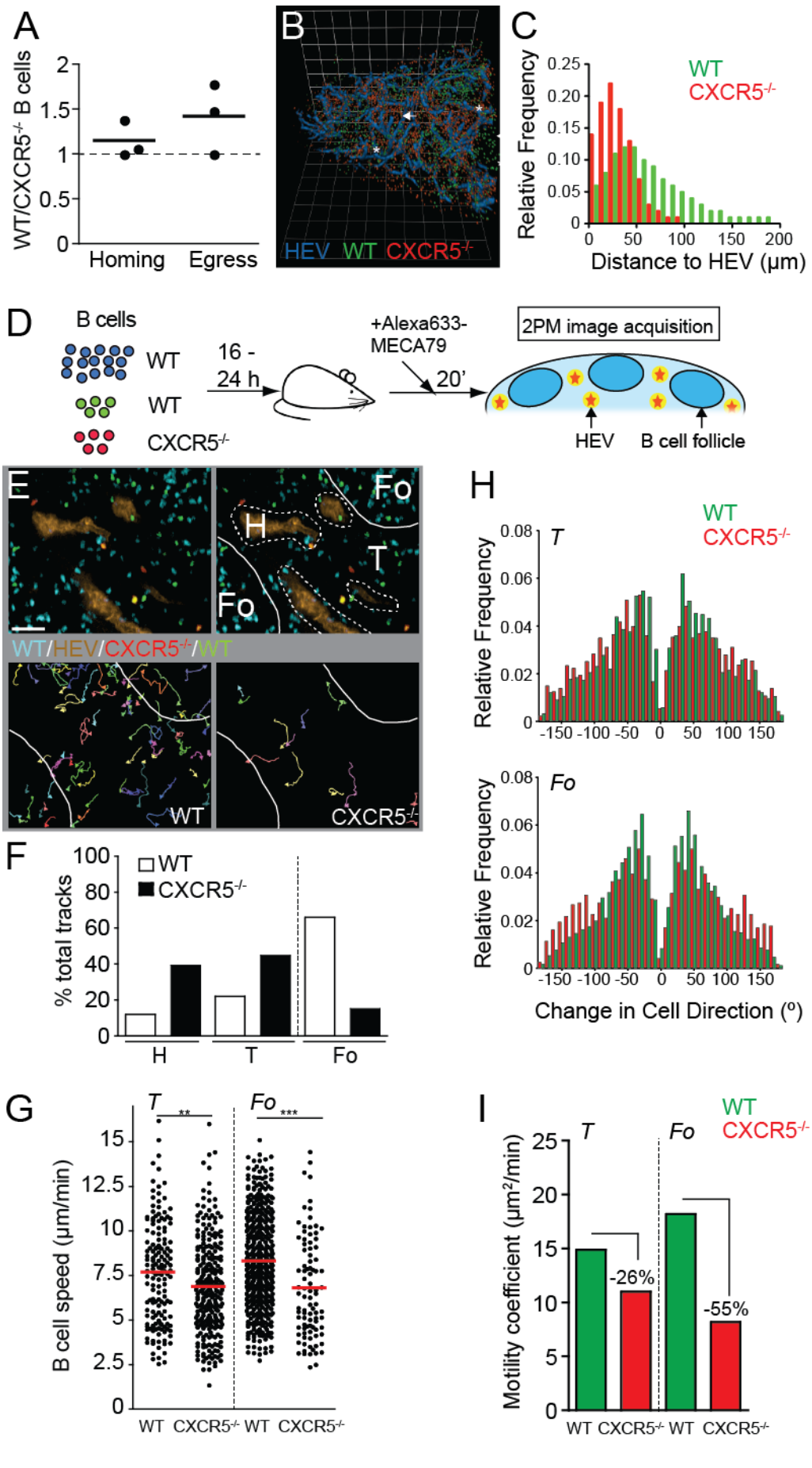
A
WT/CXCR5-/- B cells
Homing
Egress
B
HEV WT CXCR5-/-
C
Relative Frequency
WT
CXCR5-/-
Distance to HEV (µm)
D
B cells
WT
WT
CXCR5-/-
16 - 24 h
+Alexa633-MECA79
20'
2PM image acquisition
HEV
B cell follicle
E
H
T
Fo
WT/HEV/CXCR5-/-/WT
WT
CXCR5-/-
F
% total tracks
WT
CXCR5-/-
H
T
Fo
G
T
Fo
B cell speed (µm/min)
WT CXCR5-/- WT CXCR5-/-
H
T
Fo
WT
CXCR5-/-
Relative Frequency
Change in Cell Direction (°)
I
T
Fo
WT
CXCR5-/-
Motility coefficient (µm²/min)
-26%
-55%
WT CXCR5-/- WT CXCR5-/-

Figure 1

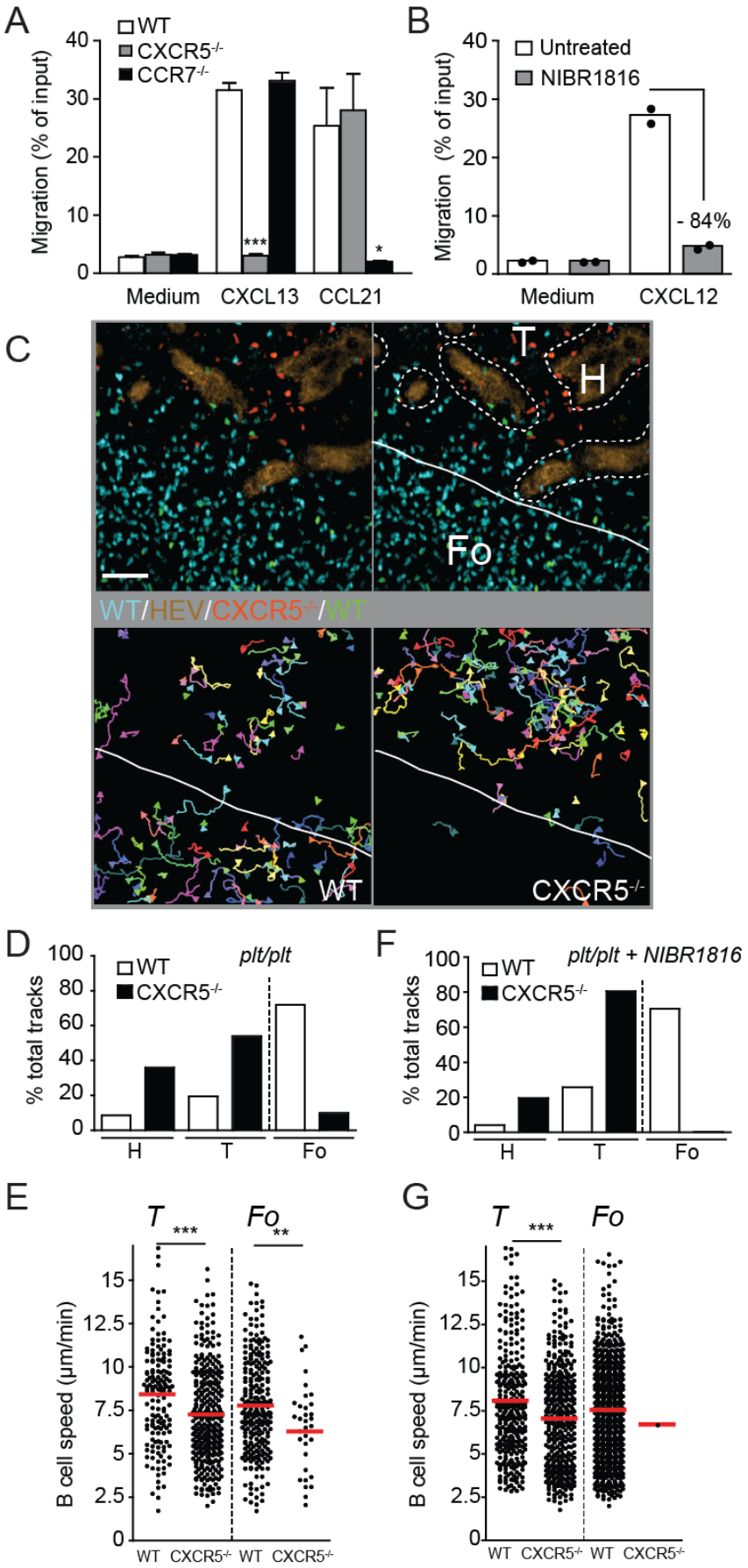
A
WT
CXCR5-/-
CCR7-/-
Migration (% of input)
40
30
20
10
0
***
*
Medium
CXCL13
CCL21
B
Untreated
NIBR1816
Migration (% of input)
- 84%
Medium
CXCL12
C
T
H
Fo
WT/HEV/CXCR5-/-/WT
WT
CXCR5-/-
D
plt/plt
WT
CXCR5-/-
% total tracks
H
T
Fo
F
plt/plt + NIBR1816
WT
CXCR5-/-
% total tracks
H
T
Fo
E
T
Fo
***
**
B cell speed (µm/min)
WT
CXCR5-/-
WT
CXCR5-/-
G
T
Fo
***
B cell speed (µm/min)
WT
CXCR5-/-
WT
CXCR5-/-

Figure 2

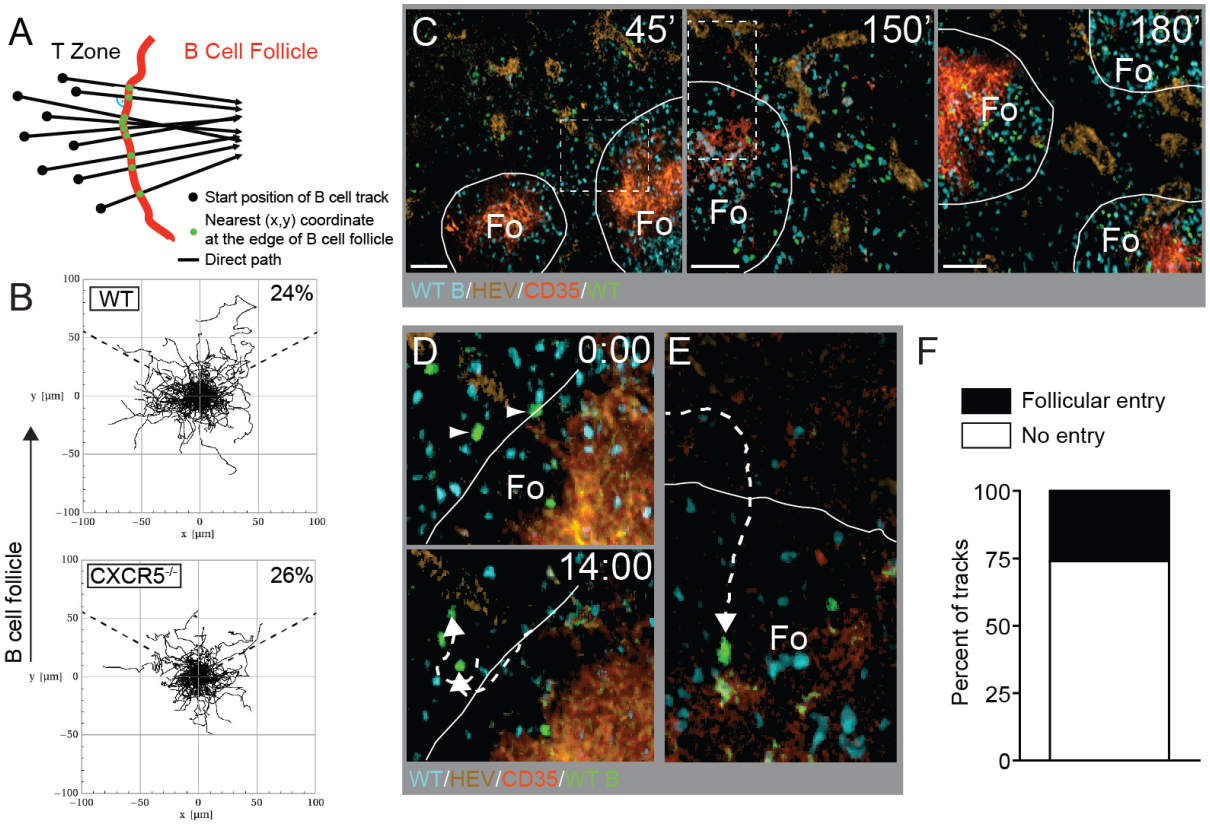
A
T Zone
B Cell Follicle
Start position of B cell track
Nearest (x,y) coordinate
at the edge of B cell follicle
Direct path
B
WT
24%
CXCR5-/-
26%
B cell follicle
y [µm]
x [µm]
C
45'
150'
180'
Fo
WT B/HEV/CD35/WT
D
0:00
14:00
E
WT/HEV/CD35/WT B
F
Follicular entry
No entry
Percent of tracks
100
75
50
25
0

Figure 3

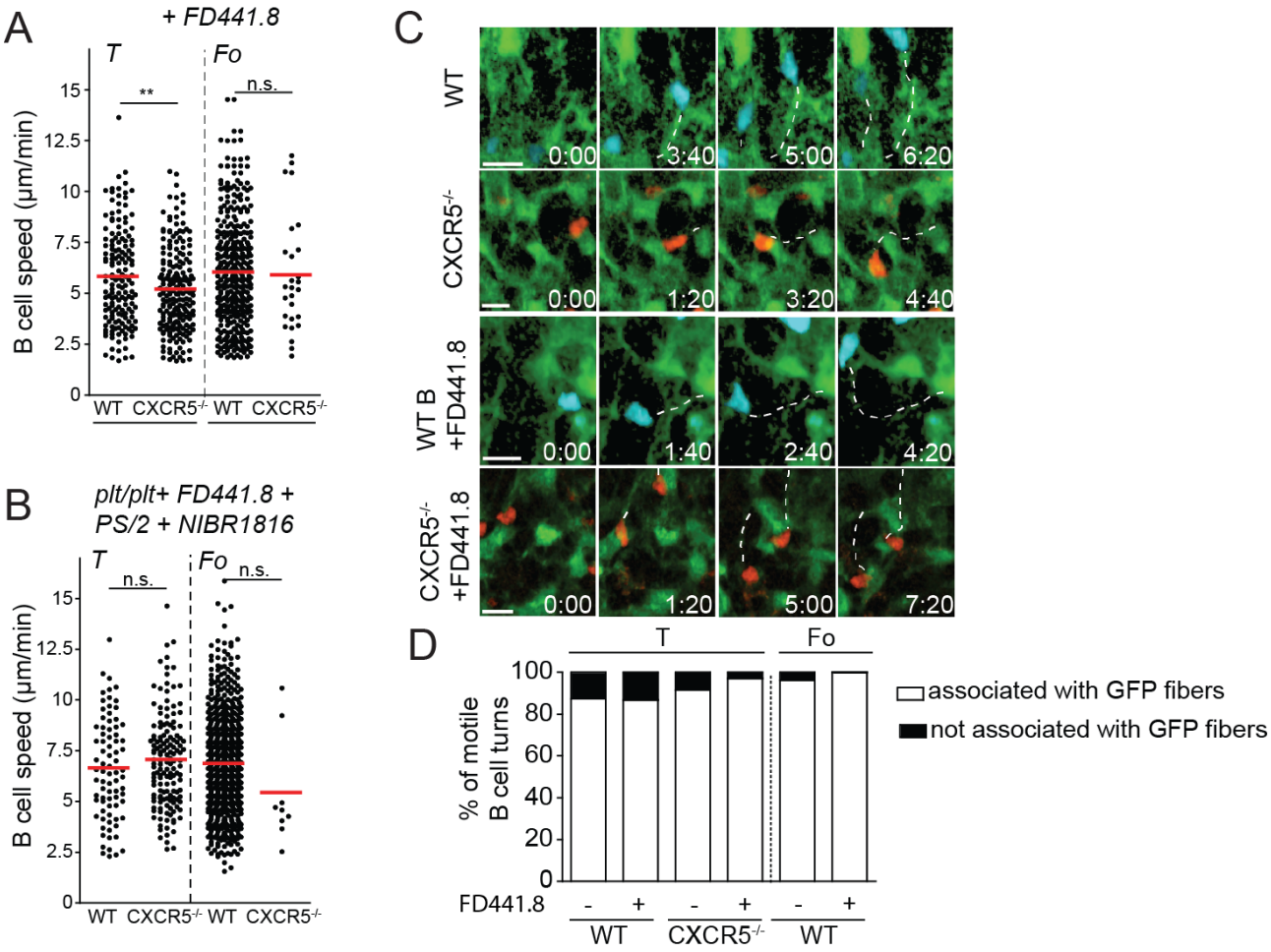
A
+ FD441.8
T
Fo
**
n.s.
B cell speed (µm/min)
WT CXCR5-/- WT CXCR5-/-
B
plt/plt+ FD441.8 +
PS/2 + NIBR1816
n.s.
n.s.
C
WT
CXCR5-/-
WT B +FD441.8
CXCR5-/- +FD441.8
0:00
3:40
5:00
6:20
1:20
3:20
4:40
1:40
2:40
4:20
7:20
D
% of motile B cell turns
associated with GFP fibers
not associated with GFP fibers
FD441.8
WT
CXCR5-/-

Figure 4

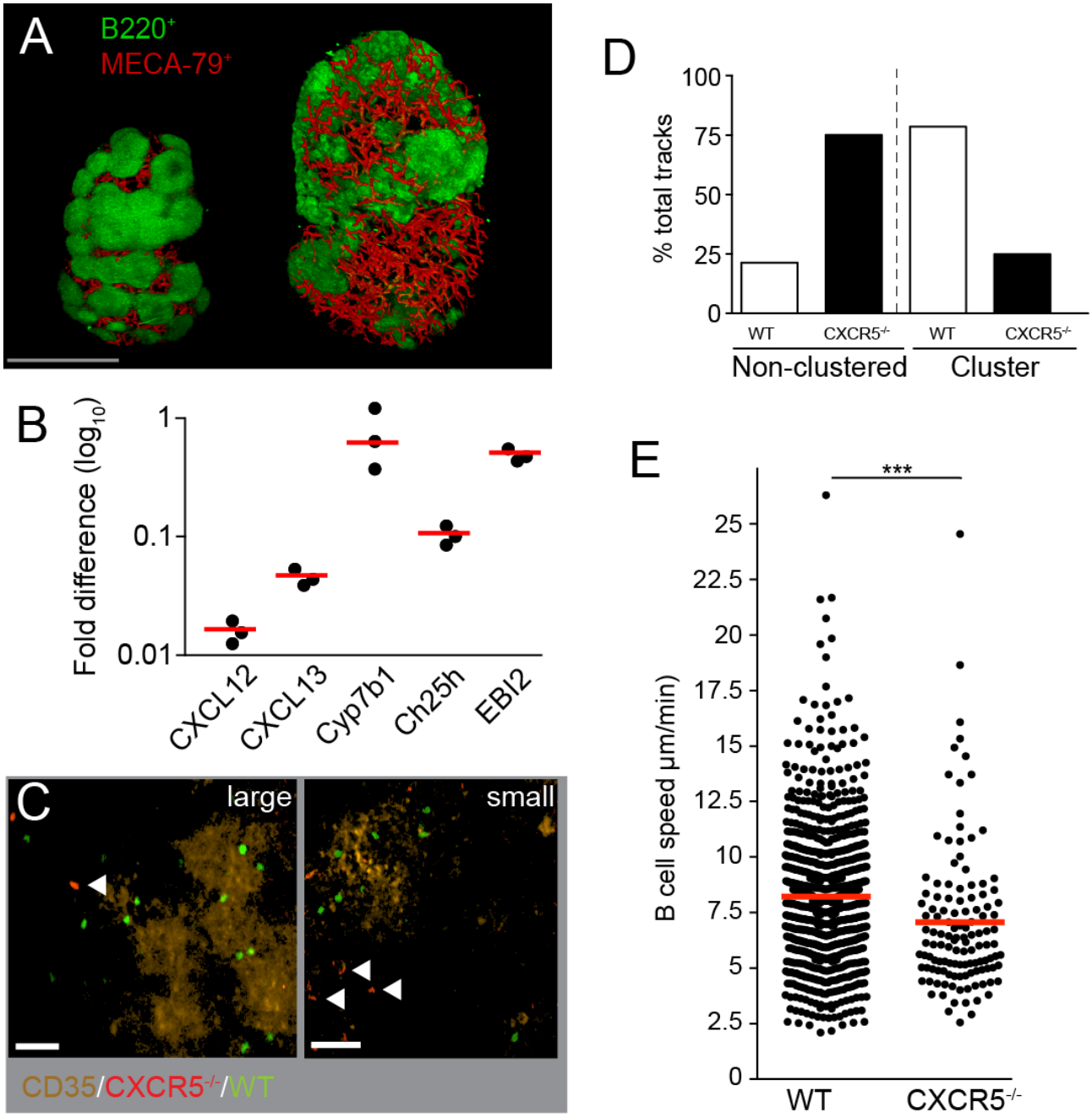
A
B220+
MECA-79+
B
Fold difference (log10)
1
0.1
0.01
CXCL12
CXCL13
Cyp7b1
Ch25h
EBI2
C
large
small
CD35/CXCR5-/-/WT
D
% total tracks
100
75
50
25
0
WT
CXCR5-/-
WT
CXCR5-/-
Non-clustered
Cluster
E
***
B cell speed µm/min)
25
22.5
20
17.5
15
12.5
10
7.5
5
2.5
0
WT
CXCR5-/-

Figure 5